

Technical Note: Drifting versus anchored flux chambers for measuring
greenhouse gas emissions from running waters

Andreas Lorke^{1*}, Pascal Bodmer^{2,3}, Christian Noss¹, Zeyad Alshboul¹, Matthias
Koschorreck⁴, Celia Somlai-Haase¹, David Bastviken⁵, Sabine Flury², Daniel F. McGinnis^{2,6},
Andreas Maeck⁷, Denise Müller^{8,9}, Katrin Premke^{2,10}

¹ Institute for Environmental Sciences, University of Koblenz-Landau, Fortstr. 7, 76829
Landau, Germany

² Leibniz-Institute of Freshwater Ecology and Inland Fisheries, Chemical Analytics and
Biogeochemistry, Müggelseedamm 310, 12587 Berlin, Germany

³ Institute of Biology, Freie Universität Berlin, Berlin, Germany

⁴ Helmholtz Centre for Environmental Research – UFZ, Department Lake Research,
Brückstr.3a, 39114 Magdeburg, Germany

⁵ Linköping University, Department of Thematic Studies – Environmental Change, 58183
Linköping, Sweden,

⁶ Institute F.-A. Forel, Section of Earth and Environmental Sciences, University of Geneva,
Geneva, Switzerland

⁷ Senect GmbH & Co. KG, An 44 – No. 11, 76829 Landau, Germany

⁸ Institute of Environmental Physics (IUP), Otto-Hahn-Allee 1, 28359 Bremen, Germany

⁹ Center for Tropical Marine Ecology (ZMT), Fahrenheitsstr. 8, 28359 Bremen, Germany

¹⁰ Leibniz Centre for Agricultural Landscape Research, Institute for Landscape
Biogeochemistry, Eberswalder Straße 84, 15374 Müncheberg, Germany

* Corresponding author: lorke@uni-landau.de

Abstract

1 Stream networks were recently discovered as major but poorly constrained natural greenhouse
2 gas (GHG) sources. A fundamental problem is that several measurement approaches have
3 been used without cross comparisons. Flux chambers represent a potentially powerful
4 methodological approach if robust and reliable ways to use chambers on running water can be
5 defined. Here we compare the use of anchored and freely drifting chambers on various
6 streams having different flow velocities. The study clearly shows that (1) anchored chambers
7 enhance turbulence under the chambers and thus elevate fluxes, (2) drifting chambers have a
8 very small impact on the water turbulence under the chamber and thus generate more reliable
9 fluxes, (3) the bias of the anchored chambers greatly depends on chamber design and
10 sampling conditions, and (4) there is a promising method to reduce the bias from anchored
11 chambers by using a flexible plastic foil seal to the water surface rather than having rigid
12 chamber walls penetrating into the water. Altogether, these results provide novel guidance on
13 how to apply flux chambers in running water, which will have important consequences for
14 measurements to constrain the global GHG balances.

15 1 Introduction

16 Rivers and streams have been identified as important links in the global carbon cycle. They
17 receive and transport terrestrial carbon from the land to the ocean and are also shown to be a
18 net source of greenhouse gases (GHG), i.e carbon dioxide (CO₂) and methane (CH₄)
19 (Aufdenkampe et al., 2011; Battin et al., 2008; Cole et al., 2007; Tranvik et al., 2009). In a
20 recent study, the global CO₂ emissions from rivers and streams were estimated to be 1.8±0.25
21 Gt C year⁻¹ (Raymond et al., 2013), which corresponds to 70% of the global ocean carbon
22 sink (Le Quéré et al., 2014). Due to the lack of knowledge of surface area and gas exchange
23 velocity, the smallest streams are considered as a major unknown component of regional to
24 global scale GHG emission estimates (Bastviken et al., 2011; Cole et al., 2007). Despite these
25 knowledge gaps, there are strong indications that small streams have the highest gas exchange
26 velocities (Aufdenkampe et al., 2011), highest CO₂ partial pressures (Koprivnjak et al., 2010)
27 and cover the largest fractional surface area within fluvial networks (Butman and Raymond,
28 2011). A continental-scale analysis of CO₂ efflux from streams and rivers revealed a
29 continuous decline of the fluxes with increasing size and discharge of the aquatic systems
30 (Hotchkiss et al., 2015).

31 Ecosystem-scale fluxes of CO₂ and CH₄ from running waters are often derived indirectly
32 using measured gas partial pressure in the surface water in combination with estimates of a
33 gas exchange velocity. For sparingly soluble gases, the exchange velocity is mainly controlled
34 by turbulence at the water-side of the air-water interface. In smaller rivers and streams,
35 turbulence is driven by stream velocity, depth and bottom roughness (Marion et al., 2014),
36 and the resulting gas exchange velocities are often parameterized with one or more of the
37 following terms: stream order, slope, flow velocity, discharge, width and depth (Alin et al.,
38 2011; Raymond et al., 2012; Wallin et al., 2011). In small streams, reach-scale estimates of the
39 gas exchange velocity can also be derived from gas tracer experiments, whereby a volatile

40 tracer (e.g., propane or sulfur hexafluoride) is injected upstream and the longitudinal decrease
41 of its dissolved concentration is measured (Halbedel and Koschorreck, 2013; Raymond et al.,
42 2012). For practical reasons, tracer gas injections are limited to application in small streams
43 and alternative methods suitable for a greater range of stream sizes are needed. Moreover,
44 recent studies revealed that the gas exchange velocity of CH₄ can be enhanced by
45 microbubbles (Beaulieu et al., 2012) and can therefore differ from that of the volatile tracer. To
46 better constrain ecosystem-scale estimates of GHG emissions and to improve the
47 understanding of the flux drivers in small running waters, reliable methods are required that
48 allow direct measurements.

49 As eddy-covariance (Baldocchi, 2014) measurements are not suitable for small streams, gas
50 flux chambers that float on the water surface are a straightforward and inexpensive method
51 for direct measurements of gas fluxes, and can easily be replicated over time and space
52 (Bastviken et al., 2015). The gas flux is determined from the change of the gas concentration
53 in the chamber headspace over time. Floating chambers have been frequently applied for
54 measuring gas fluxes in large rivers, reservoirs and lakes (e.g., Beaulieu et al.,
55 2014; DelSontro et al., 2011; Eugster et al., 2011).

56 Chamber measurements have been criticized because submerged chamber edges are thought
57 to disrupt the aquatic boundary layer, thereby affecting the gas exchange (Kremer et al.,
58 2003). Comparisons of floating chambers with other flux measurement techniques were
59 performed in lakes, rivers and estuaries. While some studies have reported a tendency of
60 floating chambers to yield higher fluxes than other methods (Raymond and Cole,
61 2001; Teodoru et al., 2015), others found reasonable agreement (Gålfalk et al., 2013; Cole et
62 al., 2010).

63 In streams and rivers, floating chambers have been deployed anchored at one spot (anchored
64 chambers) (Sand-Jensen and Staehr, 2012; Crawford et al., 2013), or freely drifting with the
65 water (drifting chambers) (Alin et al., 2011; Beaulieu et al., 2012). Although based on the

66 same principle, the two deployment modes have fundamental differences. Because of the
67 higher velocity difference between the chamber and the surface water, anchored chambers in
68 running waters may create additional turbulence around the chamber edges (Kremer et al.,
69 2003). If the effect of this turbulence on fluxes is minor, anchored chambers would be
70 advantageous as the area covered by the chamber can be controlled and because practical
71 work with anchored chambers is relatively simple. Drifting chambers will likely induce less
72 turbulence in the surface water, however it is difficult to control their coverage, potentially
73 resulting in spatially biased measurements. Drifting chambers are also complicated for several
74 reasons, e.g., the presence of obstacles in the streams or in terms of logistics, as the chambers
75 may travel far during measurement periods.

76 While establishing efficient methods for running water gas emissions are needed to improve
77 the global GHG budgets, progress in chamber based methods is prevented by the lack of
78 comparative assessments of anchored versus drifting chambers. In this study, we compared
79 measurements of GHG fluxes and the gas exchange velocity using drifting and anchored
80 chambers in various streams and rivers. Because chamber performance is expected to depend
81 strongly on chamber design, the field experiments were conducted using three different
82 chamber types. In laboratory experiments, we analyzed the flow field and the turbulence
83 under both anchored and drifting chambers at different flow velocities. The primary objective
84 of this study was to answer the question: Do anchored chambers produce reliable
85 measurements of localized GHG fluxes in running waters?

86 2 Methods

87 2.1 Chamber measurements in the field

88 Field measurements were conducted in nine different rivers and streams in Germany and
89 Poland using three different chambers ([Table 1](#)). All three data sets included *anchored*
90 *measurements*, where the chambers were tethered to stay at a fixed position as well as *drifting*

91 *measurements*, where the chambers were freely moving with the current. In two of the data
 92 sets (A and B), the temporal change of CO₂ and CH₄ concentration in the chamber headspace
 93 was measured on a boat using infrared gas analyzers (A: OA-ICOS gas analyzer, UGGA, Los
 94 Gatos Research Inc. USA, B: FTIR analyzer, Gasetm 4010, Gasetm, Finland). In the third
 95 data set (C), the gas concentration was measured using a built-in and low-cost CO₂ sensor
 96 (ELG, SenseAir, Sweden). The chamber used in (C) is described in detail elsewhere
 97 (Bastviken et al., 2015).

98 The chamber flux measurements were supplemented by measurements of dissolved gas
 99 concentrations (CO₂ and in data set A and B also CH₄) in the stream water and in the
 100 atmosphere ([Table 1](#)). Additional measurements include water temperature and near-surface
 101 current velocity, which was measured at selected sites within the study reaches using acoustic
 102 or electromagnetic current meters. More details on sampling and instrumentation are provided
 103 in [Appendix A](#).

104 The flux F (mmol m⁻² d⁻¹) of CO₂ (all data sets) and CH₄ (parts of data set A and B), was
 105 calculated from the observed rate of change of the mole fraction S (ppm s⁻¹) of the respective
 106 gas in the chamber using (Campeau and Del Giorgio, 2014):

$$107 \quad F = (S \cdot V / A) \cdot t_1 \cdot t_2 \quad (1)$$

108 Where V is the chamber gas volume (m³), A is the chamber area (m²), $t_1=8.64 \times 10^4$ s d⁻¹ is the
 109 conversion factor from seconds to days, and t_2 is a conversion factor from mole fraction
 110 (ppm) to concentration (mmol m⁻³) at *in-situ* temperature (T in K) and atmospheric pressure (p
 111 in Pa), according to the ideal gas law:

$$112 \quad t_2 = p / (8.31 \text{ J K}^{-1} \text{ mole}^{-1} \cdot T) \cdot 1000 \quad (2)$$

113 The gas exchange velocity of the respective gas at in-situ temperature k (m d⁻¹) was estimated
 114 from measured fluxes as:

$$115 \quad k = F / (K_H \cdot (p^{water} - p^{air})) \quad (3)$$

116 using the partial pressure of CO₂ and CH₄ in the stream water (p^{water}) and in the atmosphere
117 (p^{air}). The partial pressures were obtained by multiplication of the measured mole fraction
118 with atmospheric pressure. K_H is the temperature-dependent Henry constant (mmol m⁻³ Pa⁻¹)
119 (Goldenfum, 2011). The *in-situ* gas exchange velocities were converted to a standardized
120 (independent of temperature and gas diffusivity) exchange velocity k_{600} using the Schmidt
121 number dependence:

$$122 \quad k_{600} = k \cdot (600 / Sc)^n \quad (4)$$

123 where the temperature-dependent Schmidt numbers (Sc) of both gases were estimated
124 according to Goldenfum (2011). The Schmidt-number exponent n describes the dependence
125 of the gas exchange velocity of a particular gas on the diffusion coefficient of this gas in
126 water. We used $n=0.5$, which showed best agreement with measurements for wave-covered
127 and turbulent water surfaces (Jähne and Haußecker, 1998).

128

129 2.2 Turbulence measurements in the lab

130 The flow fields under freely drifting and anchored chambers were measured using particle
131 image velocimetry (PIV) in a 3 m long laboratory flume. The chamber type and geometry was
132 identical to the chamber in data set C ([Table 1](#)). The flow field under the drifting chamber was
133 measured for 50 repeated chamber runs (58 s cumulative velocity observations under the
134 chamber) at a mean flow velocity of 0.10 m s⁻¹, the highest flow velocity that could be
135 realized in the flume. Measurements under anchored chambers were performed for 90 s at a
136 mean flow velocity of 0.10 m s⁻¹. Additional measurements were performed at reduced mean
137 flow velocities of 0.08 and 0.06 m s⁻¹. As a reference, the undisturbed flow field without
138 chambers was measured for 90 s. Due to the limited length of the laboratory flume it was not
139 possible to measure gas fluxes or estimate the gas exchange velocities.

140 The flow fields were analyzed by illuminating neutrally buoyant seeding particles (diameter
141 of 20 μm, polyethylene) within a thin light sheet produced by a double-pulse laser

142 (DualPower 200-15, DantecDynamics) with 5 ms between pulses. The sampling frequency
143 was 7.5 Hz. Images were recorded in a $145 \times 145 \text{ mm}^2$ field of view with a charge-coupled
144 device (CCD) camera (FlowSense 4M MKII, 2048×2048 pixels, DantecDynamics). The
145 camera was inclined by 30° to the horizontal, which allowed for observing flow velocities
146 below the chamber.

147 The two-dimensional (longitudinal and vertical) flow velocities within the field of view were
148 estimated using an adaptive correlation algorithm (Dynamic Studio, DantecDynamics) with a
149 final spatial resolution of $2.6 \times 2.6 \text{ mm}^2$. The longitudinal extent of the observed flow fields
150 (433 mm for anchored and 395 mm for drifting chambers) covered the complete chamber
151 diameter and velocities are reported as a function of distance from the leading chamber edge
152 in both the anchored and the drifting deployment.

153 The turbulent kinetic energy (*TKE*) was estimated by assuming isotropy in the unresolved
154 velocity component as:

$$155 \quad TKE = \frac{3}{4} \overline{(u'^2 + w'^2)} \quad (5)$$

156 where u' and w' denote the temporal fluctuations of the longitudinal and vertical velocity
157 component, respectively, and the overbar denotes temporal averaging.

158 2.3 Statistics

159 The mean fluxes measured with anchored and drifting chambers in the respective field data
160 sets were compared using paired *t*-tests, comparisons between the data sets were performed
161 using 2-sample *t*-tests. Spearman rank correlations coefficients (r_s) were estimated when
162 testing for correlations between gas exchange velocities from anchored and drifting chambers
163 for each data set. All analyses were performed at a significance level $p < 0.05$, unless stated
164 otherwise.

165 3 Results

166 3.1 Drifting vs. anchored chamber measurements in the field

167 In all measurements, the CO₂ and CH₄ fluxes were positive, i.e. the streams were sources of
168 both gases to the atmosphere. While the mean CO₂ fluxes measured by drifting chambers did
169 not differ significantly among the data sets B and C, they were about seven-fold higher in data
170 set A ([Table 2](#)). In all data sets, anchored chamber fluxes were significantly higher than the
171 corresponding drifting chamber fluxes.

172 Gas exchange velocities k_{600} estimated from CO₂ measurements in the drifting chamber
173 deployments ($k_{600_CO2_d}$) ranged between 0.2 and 8.1 m d⁻¹. They varied widely within each
174 data set ([Table 2](#)), but in contrast to the current velocities mean values of $k_{600_CO2_d}$ did not
175 significantly differ among the data sets. In all data sets, however, k_{600} from anchored
176 chambers ($k_{600_CO2_a}$) differed significantly from that of drifting chambers ([Fig. 1A](#)). Except
177 for data set A, both were weakly correlated to each other ($r_s = 0.49$, $p=0.01$ and $r_s = 0.76$,
178 $p<0.001$ for data set B and C, respectively) ([Fig. 1B](#)). With only a few exceptions, the gas
179 exchange velocities under anchored chambers were higher than those under drifting chambers
180 with individual measurements, $k_{600_CO2_a}$ being up to 20 times higher than $k_{600_CO2_d}$. The
181 average ratio of both velocities was 2.2, 6.2 and 4.0 for data set A, B and C, respectively
182 ([Table 2](#)).

183 When both gases were measured, the gas exchange velocities estimated from CO₂ fluxes were
184 strongly correlated to those estimated from CH₄ measurements for both deployment types.

185 Small but significant differences were observed between $k_{600_CO2_d}$ and $k_{600_CH4_d}$, whereas the
186 CO₂ based estimates were on average slightly higher in data set A and lower in data set B
187 ([Fig. 1A](#)). In accordance with the CO₂ based estimates, k_{600} estimated from CH₄ was higher
188 under anchored than under drifting chambers ([Table 2](#)) and the ratio k_{600_a} / k_{600_d} did not
189 differ significantly between both gases.

190 When combining all data sets, there was no correlation between gas exchange velocities and
191 the measured current velocity for drifting chambers for either CO₂ or CH₄ ([Fig. 2A](#)).
192 However, for anchored chamber deployments, k_{600_a} was positively correlated to current speed
193 in data set A ($r_S=0.54$, $p=0.02$) and B ($r_S=0.7$, $p<0.001$). The ratio of the gas exchange
194 velocities estimated from both deployment types was positively correlated to current speed
195 when all three data sets were combined ($r_S=0.66$, $p<0.001$), but no significant correlations
196 were observed within the individual data sets ([Fig. 2B](#)).

197

198 3.2 Flow field and turbulence under chambers

199 The laboratory measurements revealed pronounced differences in the flow fields and
200 turbulence under the anchored and drifting chambers. The mean longitudinal flow velocity
201 was strongly reduced within the submerged part of the anchored chamber and increased
202 below the submerged chamber edge. Recirculating eddies were formed under the leading
203 (upstream) edge of the chamber (vector graphs of the mean velocity distributions are provided
204 in [Appendix B](#)). These eddies detached and injected turbulence below the chamber ([Fig. 3](#)).

205 The turbulent kinetic energy which was produced by the submerged edge of the anchored
206 chambers increased with increasing current speed ([Appendix B](#)). Under the drifting chambers,
207 the flow velocities were slightly enhanced below the submerged chamber edge, but no
208 recirculating eddies were formed.

209 The penetration depth of the chamber edges varied with time as the chamber moved vertically
210 on the rough water surface (see [Appendix B](#) for snapshots of instantaneous velocity
211 distributions and chamber penetration). However, at the same flow velocity the average
212 penetration depth of the anchored chamber was higher than that of the drifting chamber ([Fig.](#)
213 [3](#)).

214 4 Discussion

215 4.1 Chamber bias in anchored deployments

216 Our field observations showed consistently higher gas exchange velocities and gas fluxes
217 measured with anchored in comparison to freely drifting chambers in a variety of small
218 streams with flow velocities between 0.08 and 0.8 m s⁻¹. Detailed observations of the flow
219 field and turbulence under both types of chambers in the laboratory revealed a reduction of
220 mean flow velocity and the generation of chamber-induced turbulence due to the shedding of
221 eddies at the upstream part of the submerged edge of the anchored chamber. Under identical
222 hydraulic conditions, anchored chambers penetrated deeper into the water, which we attribute
223 to a partial diversion of the strong horizontal drag force imposed by the flow into the vertical
224 direction. In combination, horizontal current shear and deeper penetration caused an increase
225 in magnitude of chamber-induced turbulence with increasing difference in velocity between
226 the water flow and the chamber ([Fig. B1](#)). This mechanism has been suggested in previous
227 studies of floating chamber performance in water bodies, although there are mixed results
228 regarding its importance (Cole et al., 2010; Gålfalk et al., 2013; Vachon et al., 2010).

229 The laboratory observation agrees with our field measurements, where the ratio of the fluxes
230 measured with anchored and with drifting chambers was comparably small at flow velocities
231 <0.2 m s⁻¹. However, even at low flow velocities, the gas exchange velocity was enhanced by
232 more than a factor of two in the anchored deployment. At higher flow velocities (> 0.2 m s⁻¹)
233 typical for rivers and streams, chamber-induced turbulence obviously dominated the gas flux
234 into the anchored chambers.

235 The large (several-fold) potential overestimation of fluxes measured with anchored chambers
236 calls into question its suitability for application in running waters, particularly at high flow
237 rates. This agrees with the observations of Teodoru et al. (2015) who reported a linear

238 dependency of the gas exchange velocity under anchored chambers on the water velocity
239 relative to the chamber in a large river.

240 4.2 Correction methods and chamber optimization

241 The correlation of the anchored chamber gas exchange velocity with flow velocity observed
242 in our study could provide a potential means for correcting the artificial chamber flux, if the
243 corresponding drifting chamber gas exchange velocity was also a function of flow velocity.
244 However, no such correlation was present in our field observations, indicating that near-
245 surface flow velocity is a poor predictor for the gas exchange velocities in streams. Therefore,
246 it can be expected that river depth and bed roughness affect the near-surface turbulence more
247 than flow velocity (Moog and Jirka, 1999; Raymond et al., 2012).

248 As the correction of the effects of chamber-induced turbulence on measured fluxes seems
249 unlikely, it would be more reasonable to optimize the chamber design to completely avoid or
250 to at least reduce this effect. The rectangular chamber B produced the largest error, although it
251 remained unclear from our measurements whether this was caused by the geometry of the
252 chamber or by the high flow velocity in data set B. On this basis, we recommend the use of
253 more streamlined circular chambers to minimize the error under drifting conditions. Crawford
254 et al. (2013) and McMahon and Dennehy (1999) used streamlined (canoe-shaped) instead of
255 cylindrical or rectangular chambers to minimize the generation of chamber-induced
256 turbulence at the upstream chamber edge during anchored chamber deployments. However,
257 they did not provide evidence that this goal was reached.

258 Another approach to minimize the bias of anchored chambers would be to design chambers
259 without submerged rigid walls. Submergence of the chamber edges can be avoided
260 completely by using a thin plastic foil which adheres to the water surface to seal the chamber
261 headspace (Fig. 4A). Laboratory (PIV) measurements of the flow field were performed under
262 a foil, mimicking a chamber deployed in anchored mode. The measurements revealed a strong

263 reduction of flow disturbances and chamber-induced turbulence ([Fig. 4](#)) in comparison to
264 both anchored and drifting chambers. Such “flying chambers” require a frame to keep the
265 chamber above the water surface, which can be supported by floats at a larger lateral distance
266 to the chamber or, in small streams, also by a fixation at the river bank.

267

268 4.3 Implications for chamber-based flux measurements

269 Our study clearly shows that anchored chambers strongly overestimate the gas flux in running
270 water and are not suited to quantify greenhouse gas fluxes in streams and rivers. One possible
271 way forward to reduce this bias while still maintaining the practical advantages of the
272 anchored chambers could be flying (anchored) chambers with flexible foil sealing at the water
273 surface. Drifting chambers provide a practical and reliable solution, although they are not free
274 of potential spatial bias. Because their measurement locations are difficult to control, their
275 trajectories may not be representative for the areal mean flux from the study reach. Regions
276 with locally enhanced turbulence, e.g., stream-reaches with large emerging roughness of the
277 river bed, cannot be surveyed with drifting chambers, however the gas exchange velocity is
278 highest at these sites (Moog and Jirka, 1999). Similarly, mean-flow trajectories may bypass
279 backwaters and regions of reduced flow velocity along the stream banks. Observations in
280 reservoirs and river impoundments revealed that the enhanced sedimentation of particulate
281 organic matter can make these zones emission hot spots (Maeck et al., 2013; DelSontro et al.,
282 2011). Anchored chamber deployments may provide a useful extension of drifting chamber
283 measurements at such sites, if the flow velocity is sufficiently small. To truly validate a
284 reliable chamber method for small streams, a multi-method comparison study, including
285 tracer additions, should be performed.

286 This study shows that flux chamber approaches to measure GHG fluxes from running waters
287 have a high potential, given sufficient knowledge about appropriate chamber design and

288 deployment approaches. Thus, flux chambers are emerging as an important method to
289 constrain greenhouse gas fluxes from stream networks.

290

291 Acknowledgments

292 Parts of this study were financially supported by the German Research Foundation (grant no.:
293 LO 1150/9-1) and conducted within the *LandScales* project (*‘Connecting processes and*
294 *structures driving the landscape carbon dynamics over scales’*) financed by the Leibniz
295 Association within the Joint Initiative for Research and Innovation (BMBF) and (partially)
296 carried out within the SMART Joint Doctorate (Science for the MAnagement of Rivers and
297 their Tidal systems) funded with the support of the Erasmus Mundus program of the European
298 Union and the Swiss National Science Foundation (Grant Nr. PA00P2_142041). The
299 development and production of the chambers with built in CO₂ loggers (data set C) was
300 supported by the Swedish Research Council VR. Funding for an initial workshop was carried
301 out by the IGB cross-cutting research domain ‘Aquatic Boundaries and Linkages’. We
302 gratefully acknowledge the financial support of German Academic Exchange Service
303 (DAAD) (Sustainable water management Program (NAWAM), Grant number: A/12/91768).
304 We thank Simone Langhans for her fruitful input, which shaped the core idea of the presented
305 study. Finally, we thank the two anonymous reviewers for constructive inputs that improved
306 the manuscript.

307

308 Appendices

309 Appendix A: Additional information on the field data sets

310 A1: Data set A

311 Field measurements of five streams in North Central European Plains in Germany and Poland
312 were conducted during October 2014. Gaseous CO₂ and CH₄ emissions were measured at the
313 water-air interface with a drifting chamber attached to an Ultraportable Greenhouse Gas
314 Analyzer (UGGA; Los Gatos Research, Inc., USA). The chamber was connected to the
315 UGGA placed in a boat via two gas tight tubes (Tygon 2375), creating a circulation of air
316 being sucked in and pumped out. For the anchored measurements, we tethered the chamber to
317 a rack in the middle of the respective stream, in which we placed the sensors for continuously
318 dissolved CO₂ and CH₄ measurements (HydroC™; CONTROS Systems & Solutions GmbH,
319 Germany). Subsequently, we floated down a predefined stream section with the same
320 chamber following freely the boat or vice versa at the speed of the current. During the
321 chamber measurements, the UGGA continuously measured the gaseous CO₂ and CH₄
322 accumulation in the chamber (frequency 1 s). Flow velocity was measured with an Acoustic
323 Digital Current Meter (OTT, Germany).

324

325 A2: Data set B

326 Measurements were performed on the Bode River between Egelin-Nord and Staßfurt on 7
327 April 2014 (summer base flow 7.7 m³ s⁻¹) and 12 March 2015 (winter high flow 12.8 m³ s⁻¹).
328 The flux of CO₂ and CH₄ between water and atmosphere was measured by a rectangular
329 floating chamber, which was connected to an FTIR analyzer (GASMET 4010, Finland).
330 Measurements were performed from a boat while drifting down the river. For a single
331 measurement, the chamber was placed at the water surface for up to five minutes and CO₂ and

332 CH₄ change inside the chamber was measured every 30 s. To compare drifting and fixed
333 chamber measurements, the boat was then stopped by an anchor and measurements continued
334 for another 3-5 min. During this stationary measurement, current velocity was measured with
335 an electromagnetic current meter (MF-Pro, Ott, Germany) and water temperature were
336 measured by hand held probes (ProfiLine Multi, WTW, Germany).

337 The concentration of CO₂ in the water was continuously measured by a submersible probe
338 (HydroC™; CONTROS Systems & Solutions GmbH, Germany). Additionally samples for
339 CH₄ analysis were taken in plastic syringes and later analyzed by headspace GC.

340 Water temperature was continuously measured by temperature loggers (Tidbit, Onset,
341 U.S.A.). The barometric pressure was recorded by the FTIR analyzer.

342 Under drifting conditions the CH₄ flux was often below the detection limit while there was
343 always a positive CH₄ flux in anchored chamber deployments.

344

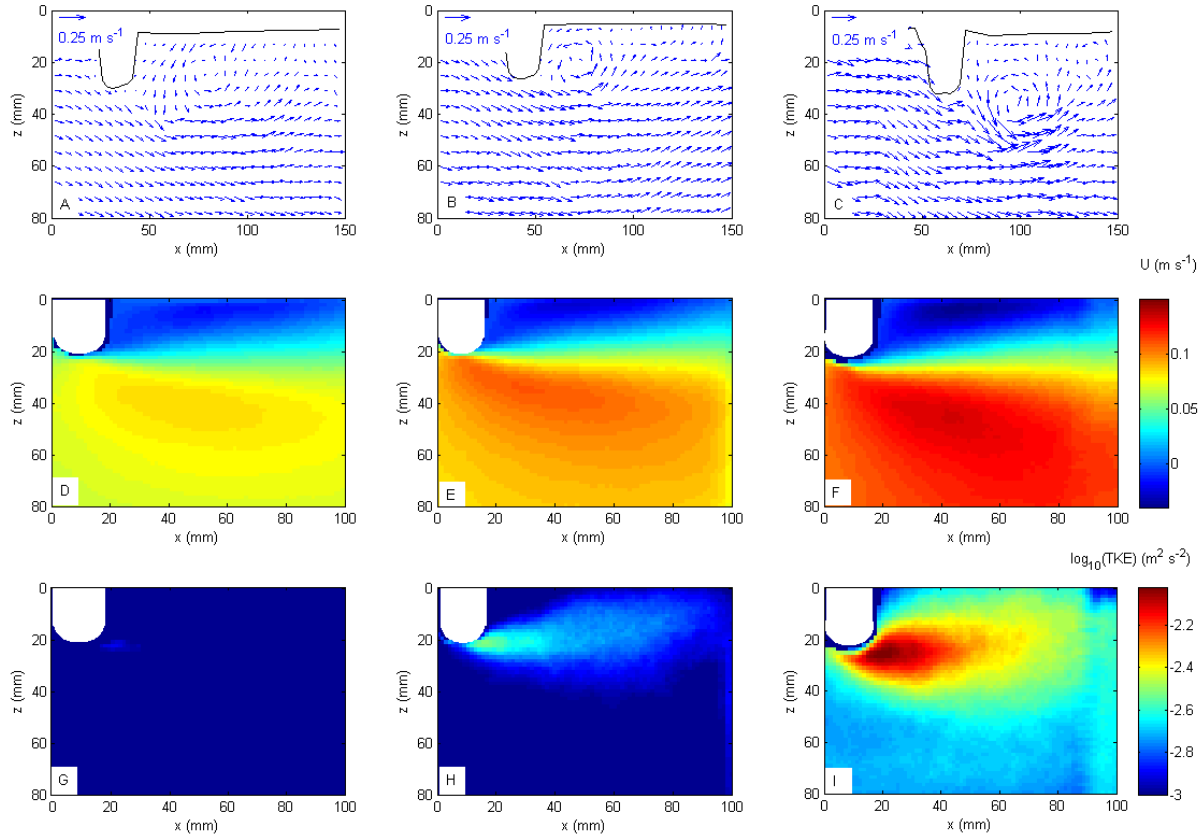
345 A3: Data set C

346 Chambers with a cross-sectional area of 0.066 m² and volume of 6.8 L were covered by
347 aluminum foil to reduce the internal heating and equipped with a Styrofoam material to keep
348 the chamber body floating on water surface. The chambers were equipped with an internal
349 CO₂ logger system that is positioned inside the headspace of the chamber (Bastviken et al.,
350 2015). The non-dispersive infrared (NDIR) CO₂ logger (ELG, SenseAir, Sweden,
351 www.senseair.se) measures CO₂ in the range of 0-5000 ppm. The logger measures
352 simultaneously CO₂, temperature and relative humidity, and operates at temperature and
353 humidity of 0-50 °C and 0-99% (non-condensing conditions) respectively. The loggers were
354 calibrated by the manufacturer and operated with 9 VDC batteries. The measurement interval
355 was adjusted to be 30 s, more information of technical specifications are provided elsewhere
356 (Bastviken et al., 2015).

357 Chambers were deployed fixed at a certain position (anchored) and freely drifting. Triplicate
358 measurements were conducted during each drifting run, and three runs were conducted at
359 each site. The anchored chambers were then used for measuring the flux of CO₂ at different
360 locations along the pathways of the drifting chambers. The chamber flux measurements were
361 supplemented by measurements of dissolved gas CO₂ and CH₄ concentrations in the stream
362 waters at each anchored stations for each run. Continuous measurements of CO₂ and methane
363 in the middle of the stream were conducted using a membrane equilibrator (Liqui-Cel
364 MiniModule, Membrana, USA) connected with an Ultraportable Greenhouse Gas Analyzer
365 (UGGA; Los Gatos Research, Inc., USA). The water samples were pumped through the
366 membrane contactor using a peristaltic pump at a constant flow rate.

367

368 Appendix B: Mean flow and turbulence under anchored chambers at different
369 current speeds






370

371 **Fig. B1:** Laboratory measurements of flow velocity and turbulence under anchored chambers
372 at different mean current speeds (left: 0.06 m s^{-1} , middle: 0.08 m s^{-1} , right: 0.10 m s^{-1} . A-C)
373 shows examples of instantaneous velocities around the leading edge of the chambers. The
374 water surface and the leading chamber edge are marked by solid black lines. D-F) temporal
375 mean longitudinal flow velocity (U). G-I) mean turbulent kinetic energy (TKE). The chamber
376 edges are masked out (white) and regions without sufficient observations ($< 90\text{ s}$ for the
377 anchored cases) are displayed in dark blue. The direction of flow was from left to right, x and
378 z refer to longitudinal distance and depth, respectively.

379 Tables

380 Table 1

381 **Table 1:** Summary of the three data sets obtained in field measurements. Pictures show the
 382 three different chambers used for the anchored and drifting approach. Additional information
 383 about the sampling procedures are provided in the [Supplementary Information](#).

Data set	A	B	C
			
Site	5 different streams North-Central European Plains in Germany and Poland	Bode river, Harz mountains, Central Germany	3 different streams, Upper Rhine Valley, South-West Germany
Chamber volume (m ³)	0.0168	0.0147	0.0068
Chamber area (m ²) (shape)	0.126 (circular)	0.098 (rectangular)	0.066 (circular)
Chamber height (m)	0.175	0.15	0.13
Penetration depth (m)	0.018	0.023	0.025
Chamber gas measurement	LosGatos, CO ₂ , CH ₄ on boat	FTIR analyzer (GASMET, Finland) on boat	Built-in low-cost CO ₂ logger (ELG by SenseAir, Sweden)
Dissolved gas measurement	Contros CO ₂ and CH ₄	Contros CO ₂ , CH ₄ with GC	UGGA with membrane contactor
Drifting measurements	following boat or vice versa	Freely drifting while followed with boat	Freely drifting
Anchored measurements	Tethered to a rack in the middle of the stream	Tethered to anchored boat	Tethered with rope from above
Number of measurements	At 5 sites: 2-5 pairs of anchored chamber measurements (upstream) and subsequent floating chamber runs	For two different discharge situations: 10-13 pairs of subsequent drifting and anchored chamber measurements down the river using a single chamber	At 3 sites: 2-3 subsequent floating chamber runs and 5 parallel anchored chambers distributed along the trajectory of the floating chamber

384 Table 2

385 **Table 2:** Discharge rate, flow velocities, gas fluxes (F_{CO_2} , F_{CH_4}), and gas exchange velocities
386 ($k_{600_{\text{CO}_2}}$, $k_{600_{\text{CH}_4}}$) estimated from drifting (subscript d) and from anchored (subscript a)
387 chambers during the three field campaigns (A-C, cf. [Table 1](#)). Except for discharge, all values
388 are given as mean \pm standard deviation.

Data set	A	B	C
No. of samples n	$n_{\text{CO}_2}=18$ $n_{\text{CH}_4}=18$	$n_{\text{CO}_2}=27$ $n_{\text{CH}_4}=9$	$n_{\text{CO}_2}=24$ $n_{\text{CH}_4}=0$
Discharge ($\text{m}^3 \text{s}^{-1}$)	0.6 – 1.4	7.7 – 12.8	0.1 – 7.6
Flow velocity (m s^{-1})	0.21 ± 0.07	0.60 ± 0.12	0.30 ± 0.07
$F_{\text{CO}_2_{\text{a}}}$ ($\text{mmol m}^{-2} \text{day}^{-1}$)	742 ± 282	302 ± 148	103 ± 47
$F_{\text{CO}_2_{\text{d}}}$ ($\text{mmol m}^{-2} \text{day}^{-1}$)	363 ± 139	55 ± 30	49 ± 36
$k_{600_{\text{CO}_2_{\text{a}}}}$ (m day^{-1})	6.5 ± 1.4	17 ± 6.4	4.1 ± 2.8
$k_{600_{\text{CO}_2_{\text{d}}}}$ (m day^{-1})	3.3 ± 1.1	3.2 ± 1.5	2.1 ± 2.5
$k_{600_{\text{CO}_2_{\text{a}}} / k_{600_{\text{CO}_2_{\text{d}}}}$	2.2 ± 0.9	6.2 ± 3.2	4.0 ± 5.0
$F_{\text{CH}_4_{\text{a}}}$ ($\text{mmol m}^{-2} \text{day}^{-1}$)	4.31 ± 1.35	1.55 ± 0.71	-
$F_{\text{CH}_4_{\text{d}}}$ ($\text{mmol m}^{-2} \text{day}^{-1}$)	2.12 ± 0.86	0.37 ± 0.16	-
$k_{600_{\text{CH}_4_{\text{a}}}}$ (m day^{-1})	6.0 ± 1.4	23.0 ± 10.8	-
$k_{600_{\text{CH}_4_{\text{d}}}}$ (m day^{-1})	2.9 ± 0.9	5.5 ± 2.4	-
$k_{600_{\text{CH}_4_{\text{a}}} / k_{600_{\text{CH}_4_{\text{d}}}}$	2.3 ± 1.0	4.8 ± 2.1	-

389

390 Figures

391 Figure 1

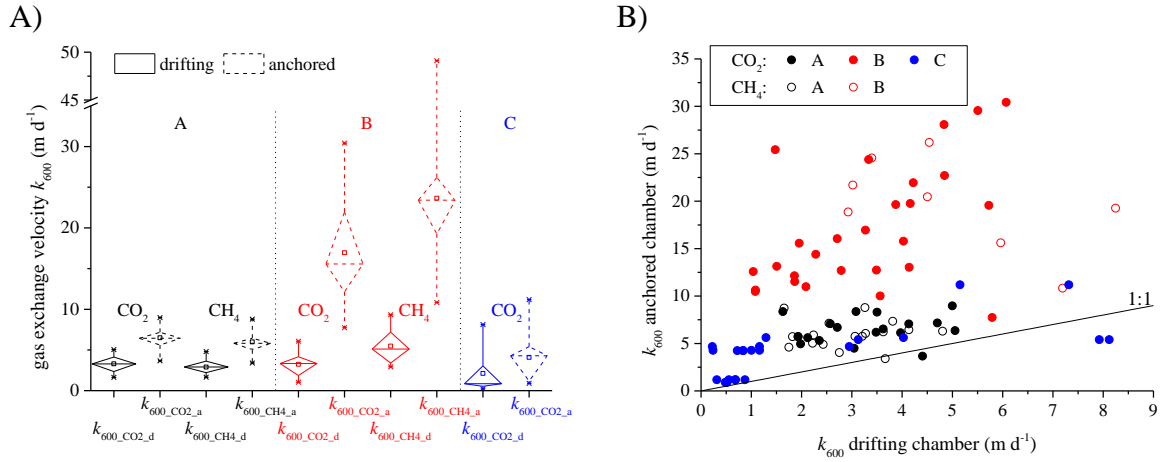
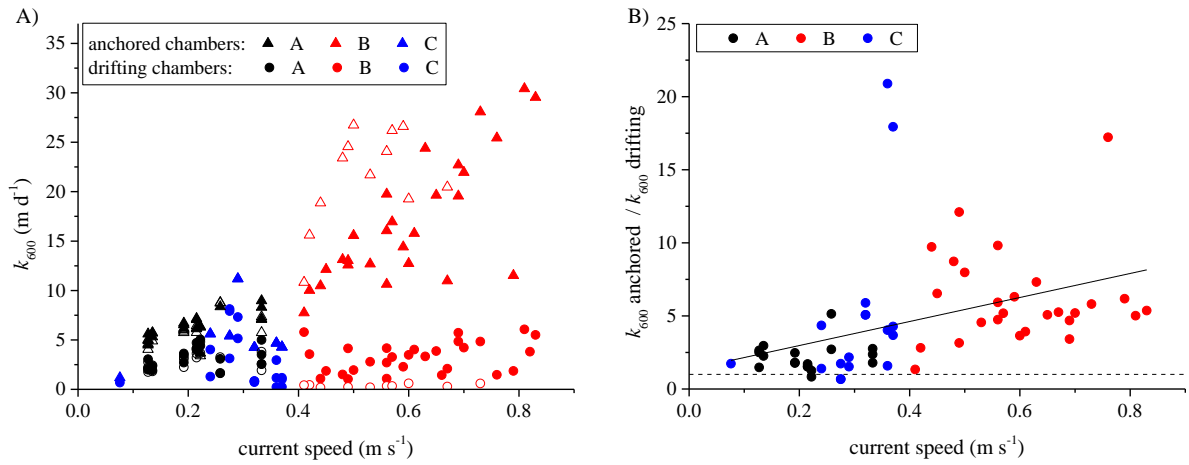


Fig. 1: A) Box plots of the standardized gas exchange (k_{600}) velocity measured using drifting (solid lines) and anchored (dashed lines) flux chambers in data set A (black), B (red) and C (blue). The diamond-shaped boxes encompass the 25-75 percentile range, whiskers show minimum and maximum, open squares and horizontal lines mark mean and median values, respectively. B) k_{600} estimated from anchored chamber deployments versus that from drifting chambers for the data sets A-C (color). Filled symbols show k_{600} estimated from CO₂ fluxes, open symbols are based on CH₄ fluxes. The solid line shows a 1:1 relationship.

392

393 Figure 2



394

395 **Fig. 2:** A) Gas exchange velocity k_{600} from anchored (triangles) and drifting (circles)

396 chambers versus current velocity for the three field data sets (A-C, colors). Filled symbols

397 show data obtained from CO₂, open symbols are based on CH₄ fluxes. B) Ratio of the gas

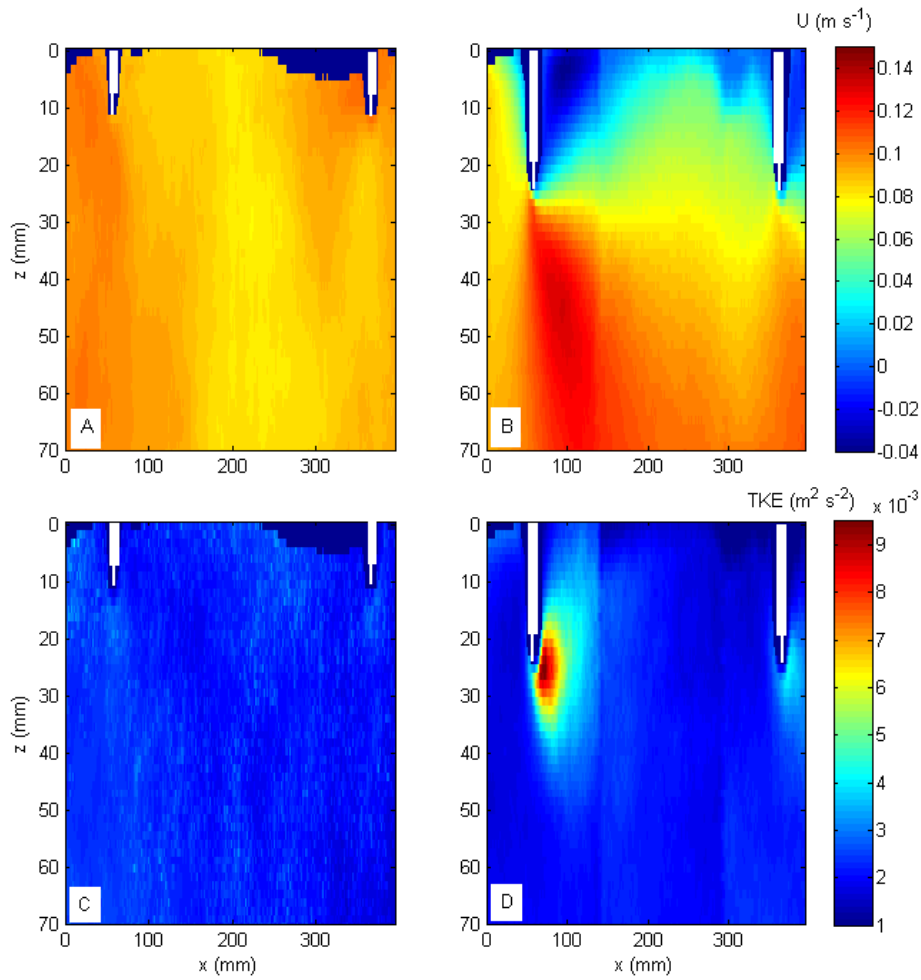
398 exchange velocities from anchored and drifting chambers versus current speed (filled

399 symbols: CO₂, open symbols: CH₄, symbol color indicates data set). The dashed line indicates

400 a constant ratio of one and the solid line shows a linear regression of the combined data sets

401 ($r_s=0.66$, $p<0.001$).

402 Figure 3



403

404 **Fig. 3:** Laboratory measurements of the mean longitudinal flow velocities (U) A) below a
405 drifting and B) below an anchored chamber. Mean turbulent kinetic energy (TKE) of the flow
406 fields below C) the drifting chamber and D) the anchored chamber. z and x refer to depth and
407 longitudinal distance respectively. Chamber edges are masked out (white) and regions without
408 sufficient observations for temporal averaging are marked by dark blue color. The flow
409 direction is from left to right and the mean flow velocity was 0.1 m s^{-1} .

410

411 Figure 4

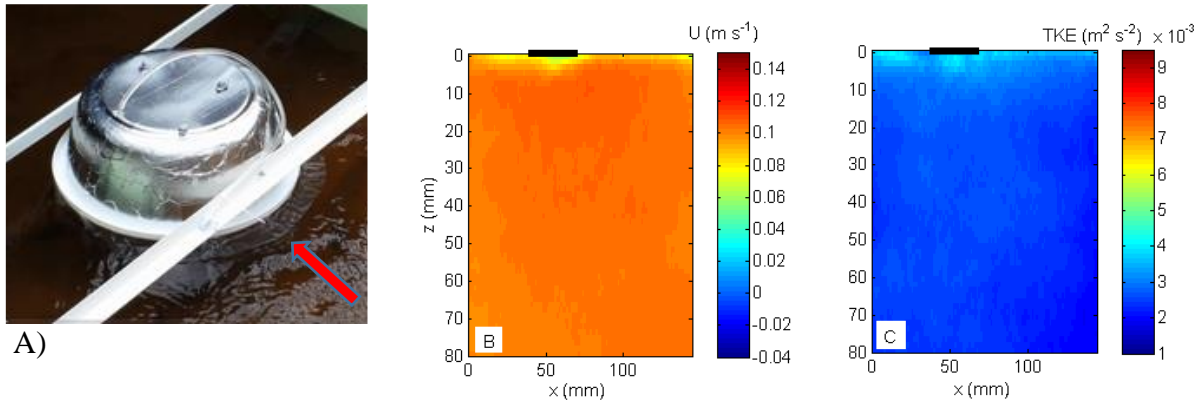


Fig. 4: A) Flying chamber design without penetration of the water surface by the chamber edges but using a plastic foil collar (marked by the red arrow) for sealing. The chamber is fixed above the water surface by a supporting frame. B) Distribution of mean longitudinal flow velocities (U) and C) turbulent kinetic energy (TKE) of the flow field below the front edge of a static foil (marked by black bar) at the water surface. The direction of flow was from left to right, x and y refer to longitudinal distance and depth, respectively. The mean flow velocity was 0.10 m s^{-1} . Color scales are identical to that of Fig. 3.

412

413 References

- 414 Alin, S. R., Rasera, M., Salimon, C. I., Richey, J. E., Holtgrieve, G. W., Krusche, A. V., and
415 Snidvongs, A.: Physical controls on carbon dioxide transfer velocity and flux in low-
416 gradient river systems and implications for regional carbon budgets, *J. Geophys. Res.-*
417 *Biogeo.*, 116, G01009, 10.1029/2010jg001398, 2011.
- 418 Aufdenkampe, A. K., Mayorga, E., Raymond, P. A., Melack, J. M., Doney, S. C., Alin, S. R.,
419 Aalto, R. E., and Yoo, K.: Riverine coupling of biogeochemical cycles between land,
420 oceans, and atmosphere, *Front. Ecol. Environ.*, 9, 53-60, 10.1890/100014, 2011.
- 421 Baldocchi, D.: Measuring fluxes of trace gases and energy between ecosystems and the
422 atmosphere – the state and future of the eddy covariance method, *Global Change Biol.*,
423 20, 3600-3609, 10.1111/gcb.12649, 2014.
- 424 Bastviken, D., Tranvik, L. J., Downing, J. A., Crill, P. M., and Enrich-Prast, A.: Freshwater
425 Methane Emissions Offset the Continental Carbon Sink, *Science*, 331, 50-50,
426 10.1126/science.1196808, 2011.
- 427 Bastviken, D., Sundgren, I., Natchimuthu, S., Reyier, H., and Gålfalk, M.: Technical Note:
428 Cost-efficient approaches to measure carbon dioxide (CO₂) fluxes and concentrations in
429 terrestrial and aquatic environments using mini loggers, *Biogeosciences*, 12, 3849-3859,
430 10.5194/bg-12-3849-2015, 2015.
- 431 Battin, T. J., Kaplan, L. A., Findlay, S., Hopkinson, C. S., Marti, E., Packman, A. I.,
432 Newbold, J. D., and Sabater, F.: Biophysical controls on organic carbon fluxes in fluvial
433 networks, *Nature Geosci.*, 1, 95-100, 10.1038/ngeo101, 2008.
- 434 Beaulieu, J. J., Shuster, W. D., and Rebolz, J. A.: Controls on gas transfer velocities in a
435 large river, *J. Geophys. Res.-Biogeo.*, 117, G02007, 10.1029/2011jg001794, 2012.
- 436 Beaulieu, J. J., Smolenski, R. L., Nietch, C. T., Townsend-Small, A., and Elovitz, M. S.: High
437 Methane Emissions from a Midlatitude Reservoir Draining an Agricultural Watershed,
438 *Environ. Sci. Technol.*, 48, 11100-11108, 10.1021/es501871g, 2014.
- 439 Butman, D., and Raymond, P. A.: Significant efflux of carbon dioxide from streams and
440 rivers in the United States, *Nature Geosci.*, 4, 839-842, 2011.
- 441 Campeau, A., and Del Giorgio, P. A.: Patterns in CH₄ and CO₂ concentrations across boreal
442 rivers: Major drivers and implications for fluvial greenhouse emissions under climate
443 change scenarios, *Glob Chang Biol*, 20, 1075-1088, 2014.
- 444 Cole, J. J., Prairie, Y. T., Caraco, N. F., McDowell, W. H., Tranvik, L. J., Striegl, R. G.,
445 Duarte, C. M., Kortelainen, P., Downing, J. A., Middelburg, J. J., and Melack, J.:
446 Plumbing the global carbon cycle: Integrating inland waters into the terrestrial carbon
447 budget, *Ecosystems*, 10, 171-184, 10.1007/s10021-006-9013-8, 2007.
- 448 Cole, J. J., Bade, D. L., Bastviken, D., Pace, M. L., and Van de Bogert, M.: Multiple
449 approaches to estimating air-water gas exchange in small lakes, *Limnol. Oceanogr.*
450 *Meth.*, 8, 285-293, 10.4319/lom.2010.8.285, 2010.
- 451 Crawford, J. T., Striegl, R. G., Wickland, K. P., Dornblaser, M. M., and Stanley, E. H.:
452 Emissions of carbon dioxide and methane from a headwater stream network of interior
453 Alaska, *J. Geophys. Res.-Biogeo.*, 118, 482-494, 10.1002/jgrg.20034, 2013.
- 454 DelSontro, T., Kunz, M. J., Kempter, T., Wüest, A., Wehrli, B., and Senn, D. B.: Spatial
455 Heterogeneity of Methane Ebullition in a Large Tropical Reservoir, *Environ. Sci.*
456 *Technol.*, 45, 9866-9873, 10.1021/es2005545, 2011.
- 457 Eugster, W., DelSontro, T., and Sobek, S.: Eddy covariance flux measurements confirm
458 extreme CH₄ emissions from a Swiss hydropower reservoir and resolve their short-term
459 variability, *Biogeosciences*, 8, 2815-2831, 10.5194/bg-8-2815-2011, 2011.

460 Gålfalk, M., Bastviken, D., Fredriksson, S., and Arneborg, L.: Determination of the piston
461 velocity for water-air interfaces using flux chambers, acoustic Doppler velocimetry, and
462 IR imaging of the water surface, *J. Geophys. Res.-Biogeo.*, 118, 770-782,
463 10.1002/jgrg.20064, 2013.

464 Goldenfum, J. A.: *GHG Measurement Guidelines for Freshwater Reservoirs*, UNESCO/IHA,
465 London, 139 pp., 2011.

466 Halbedel, S., and Koschorreck, M.: Regulation of CO₂ emissions from temperate streams and
467 reservoirs, *Biogeosciences*, 10, 7539-7551, 10.5194/bg-10-7539-2013, 2013.

468 Hotchkiss, E. R., Hall Jr, R. O., Sponseller, R. A., Butman, D., Klaminder, J., Laudon, H.,
469 Rosvall, M., and Karlsson, J.: Sources of and processes controlling CO₂ emissions
470 change with the size of streams and rivers, *Nature Geosci.*, 8, 696-699,
471 10.1038/ngeo2507, 2015.

472 Jähne, B., and Haußecker, H.: Air-water gas exchange, *Ann. Rev. Fluid Mech.*, 30, 443-468,
473 1998.

474 Koprivnjak, J. F., Dillon, P. J., and Molot, L. A.: Importance of CO₂ evasion from small
475 boreal streams, *Global Biogeochem. Cycles*, 24, Gb4003, 10.1029/2009gb003723, 2010.

476 Kremer, J. N., Nixon, S. W., Buckley, B., and Roques, P.: Technical Note: Conditions for
477 Using the Floating Chamber Method to Estimate Air-Water Gas Exchange, *Estuaries*, 26,
478 985-990, 10.1007/BF02803357, 2003.

479 Le Quéré, C., Peters, G. P., Andres, R. J., Andrew, R. M., Boden, T. A., Ciais, P.,
480 Friedlingstein, P., Houghton, R. A., Marland, G., Moriarty, R., Sitch, S., Tans, P., Arneeth,
481 A., Arvanitis, A., Bakker, D. C. E., Bopp, L., Canadell, J. G., Chini, L. P., Doney, S. C.,
482 Harper, A., Harris, I., House, J. I., Jain, A. K., Jones, S. D., Kato, E., Keeling, R. F.,
483 Klein Goldewijk, K., Körtzinger, A., Koven, C., Lefèvre, N., Maignan, F., Omar, A.,
484 Ono, T., Park, G. H., Pfeil, B., Poulter, B., Raupach, M. R., Regnier, P., Rödenbeck, C.,
485 Saito, S., Schwinger, J., Segschneider, J., Stocker, B. D., Takahashi, T., Tilbrook, B., van
486 Heuven, S., Viovy, N., Wanninkhof, R., Wiltshire, A., and Zaehle, S.: Global carbon
487 budget 2013, *Earth Syst. Sci. Data*, 6, 235-263, 10.5194/essd-6-235-2014, 2014.

488 Maeck, A., DelSontro, T., McGinnis, D. F., Fischer, H., Flury, S., Schmidt, M., Fietzek, P.,
489 and Lorke, A.: Sediment trapping by dams creates methane emission hotspots, *Environ.*
490 *Sci. Technol.*, 47, 8130-8137, 2013.

491 Marion, A., Nikora, V., Puijalón, S., Bouma, T., Koll, K., Ballio, F., Tait, S., Zaramella, M.,
492 Sukhodolov, A., O'Hare, M., Wharton, G., Aberle, J., Tregnaghi, M., Davies, P., Nepf,
493 H., Parker, G., and Statzner, B.: Aquatic interfaces: a hydrodynamic and ecological
494 perspective, *J. Hydraul. Res.*, 1-15, 10.1080/00221686.2014.968887, 2014.

495 McMahan, P. B., and Dennehy, K. F.: N₂O emissions from a nitrogen-enriched river,
496 *Environ. Sci. Technol.*, 33, 21-25, 10.1021/es980645n, 1999.

497 Moog, D., and Jirka, G.: Stream Reaeration in Nonuniform Flow: Macroroughness
498 Enhancement, *J. Hydraul. Eng.*, 125, 11-16, doi:10.1061/(ASCE)0733-
499 9429(1999)125:1(11), 1999.

500 Raymond, P. A., and Cole, J. J.: Gas exchange in rivers and estuaries: Choosing a gas transfer
501 velocity, *Estuaries*, 24, 312-317, 10.2307/1352954, 2001.

502 Raymond, P. A., Zappa, C. J., Butman, D., Bott, T. L., Potter, J., Mulholland, P., Laursen, A.
503 E., McDowell, W. H., and Newbold, D.: Scaling the gas transfer velocity and hydraulic
504 geometry in streams and small rivers, *Limnology & Oceanography: Fluids &
505 Environments*, 2, 41-53, 10.1215/21573689-1597669, 2012.

506 Raymond, P. A., Hartmann, J., Lauerwald, R., Sobek, S., McDonald, C., Hoover, M.,
507 Butman, D., Striegl, R., Mayorga, E., Humborg, C., Kortelainen, P., Durr, H., Meybeck,
508 M., Ciais, P., and Guth, P.: Global carbon dioxide emissions from inland waters, *Nature*,
509 503, 355-359, 10.1038/nature12760, 2013.

510 Sand-Jensen, K., and Staehr, P.: CO₂ dynamics along Danish lowland streams: water–air
511 gradients, piston velocities and evasion rates, *Biogeochemistry*, 111, 615-628,
512 10.1007/s10533-011-9696-6, 2012.

513 Teodoru, C. R., Nyoni, F. C., Borges, A. V., Darchambeau, F., Nyambe, I., and Bouillon, S.:
514 Dynamics of greenhouse gases (CO₂, CH₄, N₂O) along the Zambezi River and major
515 tributaries, and their importance in the riverine carbon budget, *Biogeosciences*, 12, 2431-
516 2453, 10.5194/bg-12-2431-2015, 2015.

517 Tranvik, L. J., Downing, J. A., Cotner, J. B., Loiselle, S. A., Striegl, R. G., Ballatore, T. J.,
518 Dillon, P., Finlay, K., Fortino, K., Knoll, L. B., Kortelainen, P. L., Kutser, T., Larsen, S.,
519 Laurion, I., Leech, D. M., McCallister, S. L., McKnight, D. M., Melack, J. M., Overholt,
520 E., Porter, J. A., Prairie, Y., Renwick, W. H., Roland, F., Sherman, B. S., Schindler, D.
521 W., Sobek, S., Tremblay, A., Vanni, M. J., Verschoor, A. M., von Wachenfeldt, E., and
522 Weyhenmeyer, G. A.: Lakes and reservoirs as regulators of carbon cycling and climate,
523 *Limnol. Oceanogr.*, 54, 2298-2314, 10.4319/lo.2009.54.6_part_2.2298, 2009.

524 Vachon, D., Prairie, Y. T., and Cole, J. J.: The relationship between near-surface turbulence
525 and gas transfer velocity in freshwater systems and its implications for floating chamber
526 measurements of gas exchange, *Limnol. Oceanogr.*, 55, 1723-1732,
527 10.4319/lo.2010.55.4.1723, 2010.

528 Wallin, M. B., Oquist, M. G., Buffam, I., Billett, M. F., Nisell, J., and Bishop, K. H.:
529 Spatiotemporal variability of the gas transfer coefficient ($K(\text{CO}_2)$) in boreal streams:
530 Implications for large scale estimates of CO₂ evasion, *Global Biogeochem. Cycles*, 25,
531 Gb3025, 10.1029/2010gb003975, 2011.

532